# CHARACTERIZATION OF THE FRACTURE SURFACES OBTAINED IN DIRECT TENSILE TESTS

**G. VASCONCELOS*, P.B. LOURENÇO*, M.F.M. COSTA****

***Department of Civil Engineering, Universidade do Minho**
**Campus de Azurém, 4800-058 Guimarães**
**** Department of Physics, Universidade do Minho**
**Campus de Gualtar, Braga**

**Abstract.** The study presented herein deals with an investigation of the dependence of the mode I fracture energy on the fracture path. The relief of the fracture surfaces resulting from direct tensile tests conducted on different types of granites was characterized by means of classical parameters, mean roughness and root-mean-square roughness. These parameters were obtained from the data acquired by a 3D laser topographical inspection system used to capture the texture of fracture surface profiles at various locations of the surface. A scattered linear correlation between fracture energy and the mean (micro)roughness was attained. Additionally, it was found that microstructural aspects, like planear anisotropy and grain size, as well as the weathering state, influence the fracture surface relief.

## 1. INTRODUCTION

In the tensile fracture, the transition process between micro and macrocracking states depends, on one hand, on the external applied load and, on the other hand, on the characteristics of the microstructure of the materials. In natural rocks, like granite, to which different petrographic characteristics are attributed, different interfacial mineral strengths and arrangements are expected to influence the macrocracking growth and, thus, the fracture properties, strength and fracture energy. The tensile fracture of granites with coarse grained internal structure and longer interfaces between the minerals that act as the weakest link and from which the onset of the microcracking takes place, generally leads to higher tortuosity of the fracture surfaces. In case of fine-grained granites with high strength cement matrix, the fracture surface tends to develop through minerals and smoother surfaces are achieved. Similar behavior is found in concrete where the tortuosity of the fractures surfaces is governed essentially by two aspects: the differential strength between aggregates and the cement-based matrix, and the different aggregate size. When the strength of the aggregates is higher than the cement matrix, the failure takes place in the interfaces around the inclusions. The opposite happens when the strength of the matrix prevails and cracking progress occurs through the aggregates leading to a more plane fracture surfaces and, therefore, to more brittle behavior. The increment of the aggregate size also increases the roughness of the fractures surfaces and the ductility [1-3].

In general, artificial objects exhibit a smoothly curvilinear shape and can be analyzed by the Euclidean geometry. On the contrary, due to its rough nature and irregular geometry, natural objects, like mountains, clouds and even fractures, belong to a different spatial domain, the fractal geometry. It is largely accepted that the fracture surfaces of the heterogeneous quasi-brittle materials like rocks, concrete and ceramics, by its intrinsic internal disorder due to different constituent minerals or aggregates, pores, microcraks and interfaces, are well described by fractal geometry [4-7]. The fractal structures are characterized by its similarity under different length scales, i.e., they appear identical to any degree of magnification. This property implies that any two subsequent points of the surface are not completely uncorrelated, being the degree of correlation measured by the fractal dimension *D*. It should be mentioned that the higher heterogeneity and tortuosity of the fracture surface is characterized by higher values of fractal dimension. Some recent studies have indicated that as far as fracture energy is concerned the fracture path plays a major role. Although a clear or a strong correlation between fractal dimension and fracture energy has not been found, some micro-structural aspects of the fracture surfaces could be explained by different fractal dimension values [4, 8-9]. The fractal character of the fracture energy was highlighted by Yan *et al.* [10], which pointed out a linear positive correlation between the fractal dimension and the fracture energy, meaning that a higher amount of energy is needed for the development of the fracture process on more complex surfaces. In addition to this statement, it was found that fractal dimension depends on the aggregate size: fractal dimension increases with the increase of the maximum aggregate size. Issa *et al.* [11] found a positive linear

correlation between fractal dimension and fracture toughness measured over 100 wedge-splitting specimens cast with four different maximum aggregate sizes. In addition, the dependence of the roughness surface on the fractal dimension was also evidenced, as a rougher surface corresponds to a higher fractal dimension.

In the present work, an investigation is carried out aiming at finding a correlation between roughness of the fracture surface and characteristic mechanical properties of the fracture process for distinct types of granites. The tensile mechanical properties of the granites were obtained from a comprehensive experimental program based on direct tensile tests of distinct types of granites with distinct petrographic characteristics. The post-mortem fracture surfaces of the granitic specimens were analysed by using a 3D laser topographical inspection system in order to capture the fracture surface texture profiles at various locations of the surface. Afterwards, the statistical characterization of the fracture surfaces is carried out in terms of classical quantities used in the characterization of the topography of surfaces, average roughness and root-mean-square roughness (RMS). Besides, the discussion of the correlations between fracture surface parameters and mechanical fracture parameters, the influence of the internal texture related to the preferred mineral orientation, as well as of the weathering state on the fracture path is also performed.

## 2. BRIEF DESCRIPTION OF THE GRANITES

Granite is the most used stone in the construction of ancient buildings located in the North of Portugal, either in monumental or vernacular architecture. A wide range of granitic rocks is present in masonry constructions, depending on their petrographic features, such as grain size and internal texture. Therefore, the mechanical characterization of only one type of granite would be rather limitative. In addition, the weathering processes, to which granites are subjected through years, lead to changes on the mechanical properties that require characterization. The granites used for mechanical characterization were mostly collected from the Northern region of Portugal. The selection of the granitic types was based on the mineralogical composition and grain size, aiming at providing a comprehensive sample of the Portuguese granites. In addition to these criteria, the presence of preferential orientation planes and weathering condition were also taken into account. In fact, the natural orientation planes of granitic rocks or preferred orientation of minerals (foliation) can be relevant for further analysis of the variation of the mechanical properties. Three orthogonal planes can be identified with rock splitting planes (quarry planes) defined as planes of preferred rupture. The rift plane is the plane corresponding to the easiest splitting in the quarry being easily recognized by the quarryman since it is further associated to the plane of easiest finishing. A brief description of the adopted different lithotypes is indicated in Table 1. The more weathered types of the same granite facies are distinguished with an asterisk (*).

Table 1 – Brief description of the selected granites and directions considered in the tests

| Granite designation | Petrologic description | Loading directions |
|---|---|---|
| BA | Fine to medium-grained porphyritic biotite granite | Parallel to the rift plane |
| GA, GA* | Fine to medium-grained, with porphyritic trend, two mica granite | Parallel to the rift plane |
| RM | Medium-grained biotite granite | Parallel to the rift plane |
| MC | Coarse-grained porphyritic biotite granite | Parallel to the rift plane |
| AF | Fine to medium-grained two mica granite | Parallel and perpendicular to the foliation plane |
| MDB, MDB* | Fine to medium-grained two mica granite | Parallel and perpendicular to the foliation plane |
| PTA, PTA* | Fine to medium-grained two mica granite | Parallel and perpendicular to the foliation/rift plane |
| PLA, PLA* | Medium to coarse-grained porphyritic biotite granite | Parallel and perpendicular to the rift plane |

Additionally, the loading directions considered in the experimental program are also indicated. The orientation of the rift plane was marked with the help of a quarryman and, when visible in the macroscopic scale, the foliation plane, defined from the preferential orientation of the grains, was also

marked. In case of the granite is assumed isotropic (random orientation of minerals), only the direction parallel to the rift plane was considered (granites BA, GA, GA*, RM, MC). If the granite presented visible foliation, the perpendicular and parallel directions to the foliation plane were considered (AF, MDB, MDB*, PTA). In granites PLA and PLA*, the preferred orientation of feldspar phenocrystals (flow structure) is subparallel to the rift plane and, consequently, two loading directions (parallel and perpendicular to the rift plane) were considered. As the more weathered granite PTA* does not show clear visible foliation, directions parallel and perpendicular to the rift plane were considered.

## 3. EXPERIMENTAL RESULTS

### 3.1 Fracture properties

As aforementioned, the fracture properties of the granites, namely tensile strength, $f_t$, fracture energy, $G_f$, and critical crack opening, $w_c$, were obtained based on the complete stress-displacement diagrams obtained from direct tensile tests. The size of the specimens was defined taking into consideration the restrictions of the testing equipment and the limitations for manufacturing the stone specimens. Due to the maximum distance between the platens of the CS7400S servo-controlled universal testing machine, prismatic specimens of 80mm height, 50mm length and 40mm width were considered. The adoption of a constant cross section for the specimens leads to uncertainty about the localization of the microcraks, which represents a supplementary difficulty for the control method of this type of tests, when only one Linear Variable Displacement Transducer (LVDT) as displacement control is available. Therefore, it was decided to introduce two lateral notches with a depth of 5mm at mid height of the specimen in order to localize the fracture surface. Notched specimens allow a suitable displacement control of the test through one of the four LVDTs located at the sides. However, some limitations are associated with notched specimens: the localization of the fracture zone can not be compatible with the weakest zone of the material, and the stress and deformation distribution is no longer uniform [12]. After the obtainment of the complete stress-displacements diagrams, the fracture energy was calculated as the area under the post-peak stress-crack opening displacement. The critical crack opening was defined as the displacement corresponding to the zero stress transferred between both lips of the fracture surface. The average values of the fracture properties for the distinct types of granite and the corresponding coefficient of variation are summarized in Table 2.

Table 2 – Average values of the mechanical properties for all granites. Coefficient of variation is indicated inside brackets (%)

| Granite | $f_t$ (N/mm$^2$) | $G_f$ (N/mm) | $w_c$ (mm) |
|---|---|---|---|
| BA | 8.08 (11.4) | 0.181 (14.4) | 0.087 (27.8) |
| GA | 6.01 (11.1) | 0.148 (17.7) | 0.097 (28.2) |
| GA* | 3.52 (12.3) | 0.200 (19.4) | 0.281 (32.1) |
| RM | 4.51 (9.3) | 0.153 (19.7) | 0.136 (32.2) |
| MC | 5.23 (6.3) | 0.222 (20.4) | 0.165 (30.2) |
| AF ⊥ foliation | 2.34 (11.5) | 0.179 (17.3) | 0.363 (26.4) |
| AF // foliation | 3.04 (3.0) | 0.203 (11.1) | 0.280 (29.1) |
| MDB ⊥ foliation | 2.36 (5.4) | 0.258 (16.8) | 0.484 (31.6) |
| MDB // foliation | 2.20 (4.9) | 0.250 (16.9) | 0.533 (23.8) |
| MDB* ⊥ foliation | 1.83 (4.3) | 0.270 (18.6) | 0.702 (21.0) |
| MDB* // foliation | 1.97 (5.3) | 0.249 (14.1) | 0.527 (16.0) |
| PTA ⊥ foliation | 4.15 (14.1) | 0.185 (20.2) | 0.188 (28.9) |
| PTA // foliation | 4.90 (15.6) | 0.210 (13.5) | 0.178 (22.5) |
| PTA* ⊥ rift plane | 1.56 (11.3) | 0.234 (21.0) | 0.715 (20.9) |
| PTA* // rift plane | 2.12 (4.1) | 0.255 (14.8) | 0.560 (20.9) |
| PLA ⊥ rift plane | 2.79 (10.5) | 0.145 (20.6) | 0.246 (28.5) |
| PLA // rift plane | 6.31 (13.2) | 0.266 (25.0) | 0.170 (34.0) |
| PLA* ⊥ rift plane | 1.91 (11.1) | 0.162 (20.4) | 0.422 (12.1) |
| PLA* // rift plane | 3.86 (5.1) | 0.250 (11.9) | 0.265 (25.1) |

It is observed that a wide range of variation on the fracture properties is addressed to the different types of granites. It is possible to verify that both weathering state and internal texture play an important role in the fracture behaviour of granites. The increase of the weathering means the reduction of the tensile strength and the increase on the ductility measured by the critical crack opening. The planear anisotropy reveals as a weakness plane as the tensile strength is lower in the perpendicular direction to the foliation or rift planes. This variation is particularly significant in granite PLA and PLA* characterized by flow structures oriented approximately parallel or subparallel to the rift plane. From the analysis of the critical crack opening, as an effective measure of the ductility of granites, it was stated that high strength granites appears to have a more brittle behaviour than low to medium strength granites. For a complete insight of the experimental results the reader is referred to [13].

### 3.2 Qualitative analysis of the fracture surfaces

The first assumption that the fracture energy can be related to the fracture path arises from the observation of the fracture surfaces obtained for both loading directions, regarding e.g. granites PLA and PLA*, see **Fig. 1**. For this type of granite a much more tortuous fracture surface is observed for the tensile load applied in the direction parallel to the rift plane, when compared with the rather flat surface obtained in the perpendicular direction. The internal texture, with the directional arrangement of the coarse feldspar phenocrystals, appears to be the main reason for such distinct behavior. It should be mentioned that the location of the notches in the specimens that were used in the mechanical characterization imposes that fracture plane occurs almost perpendicular to the applied load. This fact implies that different fracture features occur for both loading directions regarding the preferential alignment of the coarse feldspar megacrystals. As it was referred before, the feldspar becomes visible predominantly at the subparallel direction to the rift plane. This means that the fracture of this mineral according to its direction of alignment leads to a much more tortuous surface, which possibly implies a higher amount of energy to produce and to develop the fracture process. When the direction of loading is perpendicular to the rift plane, the splitting of the two halves becomes easier considering that the cleavage of the feldspar megacrystals according to its preferred orientation develops with less absorption of energy. Although the foliation degree exhibited by some granitic rocks (associated to the particular alignment of the biotite and muscovite minerals) is not extremely remarkable, differences are found on roughness of the respective fracture surfaces. Furthermore, in weathered granites, as the mineral interfaces becomes weaker, it is reasonable that the fracture growth occurs along these, leading to more tortuous fracture surfaces and, thus, higher values of the fracture roughness should be found.

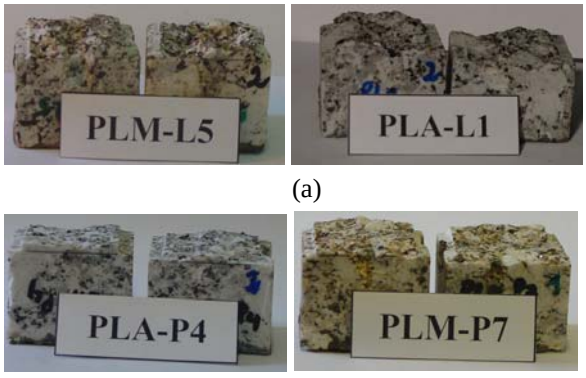


**Fig. 1** – Fracture surfaces; (a) granite PLA and PLA* loaded in the direction parallel to the rift plane; (b) granite PLA and PLA* loaded in the direction perpendicular to the rift plane

## 4. INSPECTION OF THE FRACTURE SURFACES

### 4.1 Equipment and procedure

The particular features found by simple observation of the fracture surfaces motivated a more detailed description of its texture. The quantitative analysis of the fracture surface roughness was made based on the results obtained in the inspection of the fracture surfaces of the tensile specimens by means of an

automated system of 3D topographical inspection of rough surfaces developed at the Laboratory of Microtopography of the Physics Department of University of Minho [14]. The system is based on an active optical triangulation method with mechanical sample scanning, see Fig 2. This microtopography system uses, in its usual configuration, a geometry with oblique incidence and normal observation. In order to cope with the requirements presented by the particular type of granite samples, characterized by relatively large depths up to several millimeters with steep relief structures, the geometry was changed to normal incidence with oblique observation at low angles, so that the shadowing can be reduced. A high depth of field microscope objective was used in the observation lever of the system.

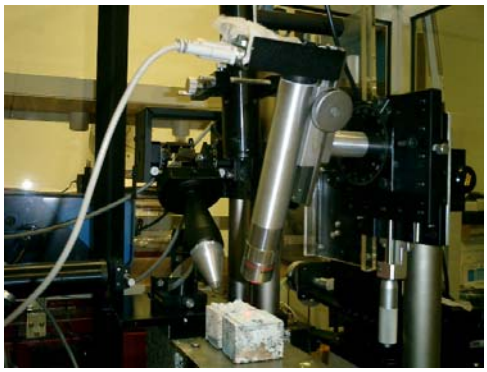

**Fig. 2** – 3D surface inspection system

The surface inspection was made on one of the cracked halves of six to height specimens, per granite type. In order to facilitate the incidence of the laser and the measurements of the height differences at each scanned point, a white coat was applied on the fracture surfaces of the specimens to be measured, see Fig 3a. According to Fig. 3b, three profiles were taken in each direction of the fracture surface, being two of them lateral and the other one central. The profile points were recorded every 10μm along the path with a resolution of 0.3μm in height. As the surface parameters are scale dependent [15] , the measurement length of the profiles should be the same for all specimens, so that the results are comparable.

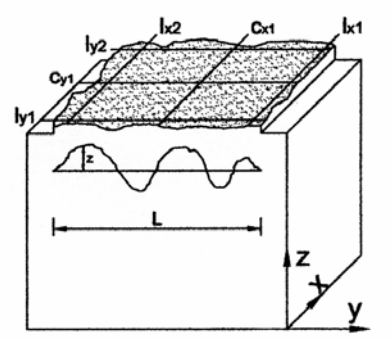


(a) (b)

**Fig. 3** – Specimens and definition of the coordinate system for acquisition; (a) preparation of the specimens for inspection; (b) definition of the acquired profiles

### 4.2 Roughness profile analysis

The first step of the fracture surface characterization is based on the determination of the standard amplitude parameters related to entire profiles. The average roughness, $r_a$, and the root-mean-square roughness (RMS), $r_q$, are given by the following expressions:

$$r_a = \frac{1}{L}\int_0^L |z(x)|\, dx \tag{1}$$

$$r_q = \sqrt{\frac{1}{L}\int_0^L z^2(x)dx} \tag{2}$$

where $z$ ($x$) is the center-line profile and $L$ is the length of the projected profile, see **Erro! A origem da referência não foi encontrada.**b. The mean values of these parameters were computed taking into account the values obtained for the six profiles defined for each specimen. The average roughness parameters for each granite type were then obtained as the average of the measured specimens. The roughness parameters for the total profile calculated according to eqs. (1, 2), designated by $P_a$ and $P_q$, are well correlated. As displayed in **Fig. 2**, the mean-root-square roughness, $P_q$, presents systematically higher values than the mean roughness, $P_a$.

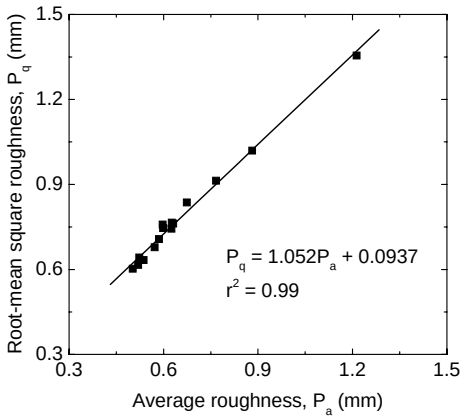


**Fig. 2** – Relation between total root-mean-square (RMS), $P_q$, and the average total roughness, $P_a$

**Fig. 3**a gives the relation between the average total roughness $P_a$ and the fracture energy. The results for the complete set of lithotypes is somewhat scattered. However, it is clear that the three granites MC, PLA* and PLA deviate from the general trend. In particular, the value of the average roughness obtained for granite MC is abnormally high, when compared with the other granites. The reason for this is the coarse feldspar megacrystals, which seems to present some degree of cleavage, as well as the clusters of quartz that are randomly spread on the fracture surface. Very high values of the roughness are also found for the granites PLA and PLA* in the parallel direction to the rift plane. If these values are excluded from the data, a reasonable linear correlation is achieved for the other granite results, see **Fig. 3**b.

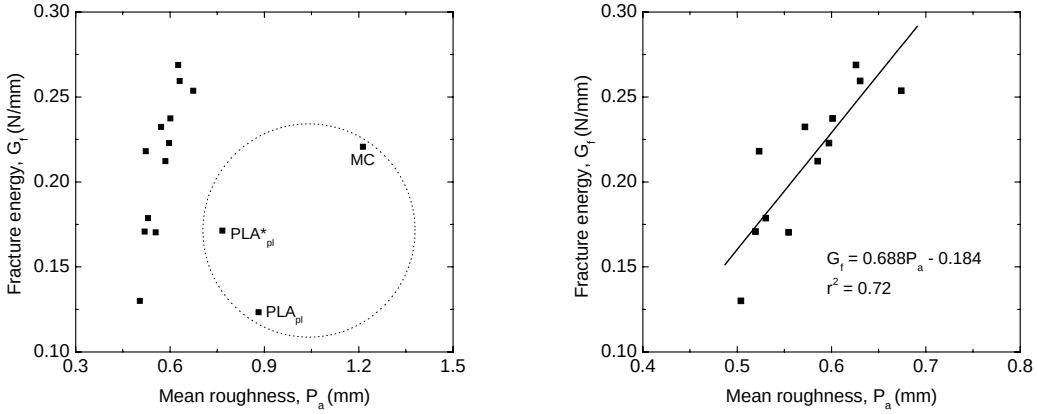


**Fig. 3** – Relation between mean roughness, $P_a$, and fracture energy, $G_f$; (a) full set of tests; (b) selected samples, without granites MC and PLA

The weak correlation between the roughness and the fracture energy led to the need of a more careful analysis of the fracture surface texture. In fact, the surface profile texture can be understood as a composition of structures with different ranges of irregularity and irregularity distribution associated to different spatial frequency ranges. The high frequency (short wavelength) components, corresponding to the finest irregularities on a surface, are repeated with low spacing and are identified as the roughness or microroughness [14]. The low frequencies or long wave components correspond to smooth changes in the profile and represent the longer spatial wavelength features of the surface, being associated with the waviness or macroroughness [14]. Although often both regimes are considered together in the characterization of the texture of the surfaces, sometimes it is advisable to separate

them, since each regime can be associated to different mechanism. Thus, a suitable moving average filtering procedure was applied to the texture profile in order to set apart the waviness from the roughness [13]. An example of the filtering of a surface texture profile is given in **Fig. 4**. This illustrates a typical S shape profile of the fracture surface attributed to a high number of granites, with the waviness and the roughness regimes presented separately. It can be observed that the long wave components (waviness) play a major role in the final geometry of the texture profile and, to some extent, command its relief. Obviously, the sum of the waviness and the roughness yields the texture profile. The identification of these distinct roughness regimes on the texture profiles obtained for the granite specimens leads to the need of clarification of the mechanisms that may lead to it. In addition, it is important to understand how the different components of the texture profile are correlated with the variation of the fracture parameters such as the fracture energy.

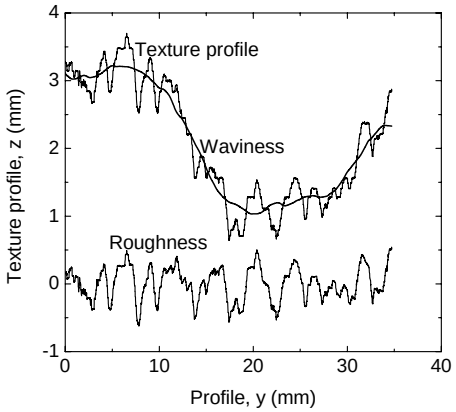


**Fig. 4** – Surface texture profile and the different roughness regimes: waviness and roughness

### 4.3 Texture parameters

After filtering the original texture profiles, the amplitude parameters regarding the waviness, $W_a$ and $W_q$, and the roughness (microroughness), $R_a$ and $R_q$, were calculated according to eqs. (1, 2) applied to the appropriate waviness and roughness profiles. The mean values of these parameters as well as the coefficients of variation inside brackets (%) corresponding to the granite types are shown in Table 3.

Table 3 – Mean values of the roughness parameters. Coefficient of variation is inside brackets (%)

| Granite | $R_a$ (mm) | $R_q$ (mm) | $W_a$ (mm) | $W_q$ (mm) |
|---|---|---|---|---|
| BA | 0.179 (13.0) | 0.236 (14.1) | 0.547 (28.0) | 0.630 (26.0) |
| GA | 0.159 (15.6) | 0.207 (14.1) | 0.415 (23.1) | 0.494 (23.3) |
| GA* | 0.190 (7.1) | 0.252 (11.0) | 0.535 (22.4) | 0.537 (22.3) |
| RM | Not measured | Not measured | Not measured | Not measured |
| MC | 0.243 (18.7) | 0.323 (20.3) | 1.105 (21.8) | 1.235 (18.7) |
| AF ⊥ foliation | Not measured | Not measured | Not measured | Not measured |
| AF // foliation | 0.170 (10.4) | 0.235 (12.2) | 0.416 (22.2) | 0.495(21.7) |
| MDB ⊥ foliation | 0.232 (9.7) | 0.309 (9.2) | 0.595 (20.1) | 0.701 (20.1) |
| MDB // foliation | 0.204 (6.4) | 0.273 (7.4) | 0.516 (21.3) | 0.605 (20.1) |
| MDB* ⊥ foliation | Not measured | Not measured | Not measured | Not measured |
| MDB* // foliation | Not measured | Not measured | Not measured | Not measured |
| PTA // foliation | 0.157 (11.4) | 0.202 (11.5) | 0.507 (19.1) | 0.593 (18.8) |
| PTA ⊥ foliation | 0.165 (6.0) | 0.216 (7.5) | 0.429 (33.6) | 0.504 (33.4) |
| PTA* ⊥ rift plane | 0.209 (20.7) | 0.284 (14.6) | 0.483 (19.9) | 0.557 (17.8) |
| PTA* // rift plane | 0.198 (10.9) | 0.261 (14.5) | 0.519 (13.7) | 0.601 (12.8) |
| PLA ⊥ rift plane | 0.155 (14.4) | 0.221 (13.5) | 0.477 (24.7) | 0.555 (23.1) |
| PLA // rift plane | 0.212 (10.9) | 0.272 (16.5) | 0.733 (22.1) | 0.859 (20.4) |
| PLA* ⊥ rift plane | 0.176 (8.6) | 0.235 (9.3) | 0.515 (16.5) | 0.608 (15.4) |
| PLA* // rift plane | 0.244 (9.8) | 0.322 (10.4) | 0.622 (14.9) | 0.728 (15.6) |

For all granites the values of the mean roughness, $R_a$, is lower than the values of the root-mean-square roughness, $R_q$, which is characteristic of rough surfaces. The values of the average surface waviness are always substantially higher than the values obtained for the roughness. This indicates that the longer space wavelength features assume an important contribution to the total texture profile surface.

### 4.4 Influence of the weathering state and internal texture on the surface roughness

The analysis of the mean values of the roughness, $R_a$ and $R_q$, regarding the fresh and weathered granites, namely GA, GA*, PTA, PTA*, PLA and PLA*, indicates that weathered granites present always higher values, see **Fig. 5**a. This fact can be explained by the alteration of the internal microstructure activated by the weathering effects. In fact, weathering not only affects the strength of the minerals, but also leads to the appearance of pores and voids that result in significant increase of the porosity. It is understandable, therefore, that if the macrocrack develops around the weakest mineral boundaries, a more tortuous fracture surface is obtained and higher values of the roughness parameters are found. In fact, the difference detected in the roughness parameters between fresh/less weathered and weathered granites is not followed by the waviness parameters. The mean values of $W_a$ and $W_q$ are higher for granite GA* than for granite GA, but the same trend does not occur for the granites PLA and PTA. This seems to indicate that microstructural changes induced by weathering are more accurately described by the variation of the finest irregularities described by the roughness parameters.

A simplified grain size mineral analysis can be performed based on the simplified petrographic description of the granites presented in Section 2. The granites were grouped as fine to medium and medium to coarse-grained. From **Fig. 5**b, it can be seen that medium to coarse-grained granites exhibit larger values of roughness parameters (around 20% higher), $R_a$ and $R_q$, and waviness parameters (around 35% higher), $W_a$ and $W_q$, in comparison with fine to medium-grained granites. This means that the increase of the grain size of the granites implies a marked increase on all the calculated roughness parameters. The difference obtained for the roughness parameters between the two groups of granites is explained by the intrinsic microstructure of medium to coarse-grained granites. In fact, the failure occurs in the interfacial zone of the different minerals, with higher surface contact, or through the minerals, with larger grain size. It is noted that part of the coarse-grained granites, such as PLA, PLA* and MC, have a porphyritic texture, which takes a major relevance on the fracture surface parameters, particularly as far the waviness parameter is concerned.

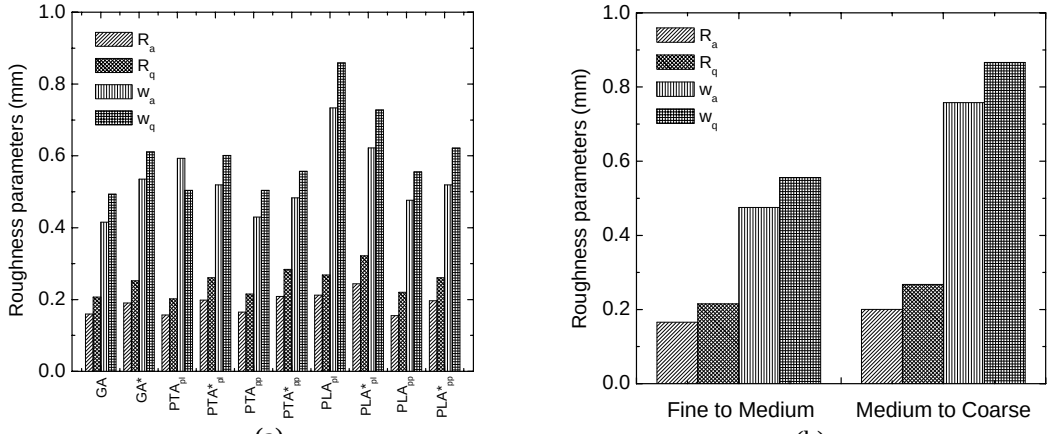


**Fig. 5** – Roughness parameters; (a) fresh vs. weathered granites; (b) effect of the grain size

The values of the roughness parameters, $R_a$ and $R_q$, depend on the direction of the fracture propagation. For granites MDB and PTA*, the roughness presents lower values when the fracture surface develops in the direction parallel to the perceptible foliation or rift planes. The interval of variation is, however, relatively small ranging between 5 and 10%. This feature seems to be in disagreement with the expected theoretical flat surface developed when tensile load is applied in the direction perpendicular to the anisotropy due to the natural alignment of the two mica minerals. As the anisotropy plane can act as a large flaw, which induces the onset of the microcracking, the fracture surface should be approximately flat when the applied load is perpendicular to the foliation. This aspect would be fully verified if the foliation plane was deeply defined. A more clear structural deviation on the texture parameters was found for the PLA and PLA* granites. All roughness parameters depend substantially

on the direction as fracture surface propagates. Both roughness and the waviness parameters exhibit higher values in the direction parallel to the rift plane. This fact confirms numerically the visual evidence that more tortuous fracture surfaces are generated in the direction parallel to the rift plane. Similarly to the anisotropy exhibited in terms of the fracture parameters, this material also presents large anisotropy regarding the roughness parameters.

### 4.5 Correlation between surface roughness and fracture energy

The mean values of the fracture energy were plotted against the mean values of the roughness and the waviness. **Fig. 6**a shows that there is a rough linear correlation between the fracture energy and the mean values of the roughness, $R_a$. The energy consumed in the crack opening process depends on the tortuosity of the fracture path that is essentially related to the finest features of the fracture surface texture. The increase of the microroughness means the increase of the consumed energy. This finding is in agreement with other results reported in literature [1, 6]. Nevertheless, it should be stressed that in the present work the fracture surfaces characterization is performed only based on the statistical average roughness. Note that the fractal dimension is also a measure of the tortuosity of the fracture surfaces and is essentially related to the high frequency components of the surface profiles. When the analysis is restricted to the granites PLA and PLA*, whose simple visual inspection of the fracture surfaces led to the present investigation, the linear fit is excellent. This relation confirms numerically the qualitative assumption that the fracture energy is largely influenced by the internal structure of this heterogeneous type of granite.

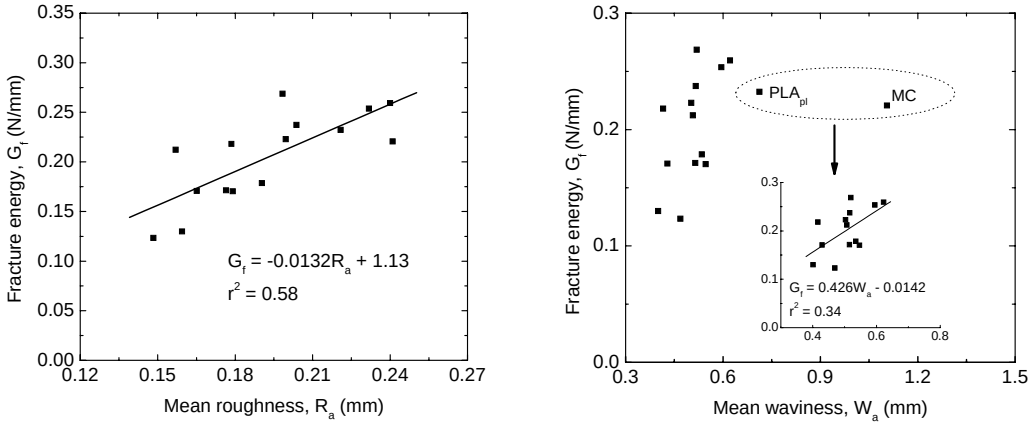


**Fig. 6** – Relation between texture properties and fracture parameters; (a) mean roughness vs. fracture energy; (b) mean waviness vs. fracture energy

**Fig. 6**b shows that no correlation was found between waviness parameter and the fracture energy. However, if the values of the waviness obtained for the granites MC and PLA in the direction parallel to the rift plane are excluded, a trend for the values of fracture energy to increase with the increase of the waviness is verified. This trend is much less significant than the relation found for the mean roughness, $R_a$. Moreover, the interaction between the texture parameters and the tensile strength was also analyzed being observed that no statistical correlation was found between the tensile strength and the roughness parameters. A similar conclusion was achieved as far as the critical crack opening is concerned. The high anisotropy exhibited by the granites PLA and PLA* can be pointed out as possible reason that disturbs any relation.

## 5. CONCLUSIONS

The qualitative information given by the observation of the fracture surfaces obtained after granite specimens had been tested under tensile loading, revealed a possible influence of microstructural aspects preferred orientation of minerals) on the fracture surface relief. This led to the need to carry out a more detailed quantitative evaluation of the surface roughness features in order to clarify the mechanisms involved in the fracture process of different types of granites. In order to evaluate the roughness of the fracture surfaces, a topographical inspection was performed by means of a laser 3D topographic inspection system, which enabled the definition of the texture profiles of the surface. The

characterization of the fracture surfaces was based on classical parameters: mean and root-mean-square roughness. A filtering procedure was applied to the total profiles so that the micro (roughness) and macro features (waviness) of the fracture surface could be highlighted. A significant achievement of this task was the proposed correlation between roughness and fracture energy. Besides, it was possible to confirm that fracture surface relief is clearly dependent on microstructural aspects, such as preferential orientation of mineral (planear anisotropy) and grain size. The weakness of the grain boundary strength associated to the increase of the weathering state means an increase of the roughness microroughness.

## 6. REFERENCES

[1] Sabir, B.B., Asili, M.W., "On the tortuosity of the fracture surface in concrete", Cement and Concrete Research, 27, 785-795 (1997).

[2] Tadesmir et al., "Combined effects of silica fume, aggregate type, and size on the post-peak response on concrete in bending", ACI Materials Journal, 96, 55-63 (1999).

[3] Rao, G.A., Prasad, B.K.R., "Fracture energy and softening behavior of high-strength concrete", Cement and Concrete Research, 32, 247-252, 2002.

[4] Chiaia B., Van Mier, J.G.M., Vervuurt, A., "Crack growth mechanisms in four different concretes: microscopic observations and fractal analysis", Cement and Concrete Research, 28, 103-114 (1998).

[5] Carpinteri, A., Chiaia, B., "Multifractal nature of concrete fracture surfaces and size effects on nominal fracture energy", Materials and Structures, 28, 435-443 (1995).

[6] Saouma, V.E., Barton, C.C., "Fractals, fractures, and size effects in concrete", Journal of Engineering Mechanics, 120, 835-854 (1994).

[7] Wang, Y., Diamond, S., "Fractal study of the fracture surfaces of cement pastes and mortars using a stereoscopic SEM method", Cement and Concrete Research, 31, 1385-1392 (2001).

[8] Chiaia, B., Vervuurt, A., Van Mier, J.G.M., "Lattice model evaluation of progressive failure in disordered particle composites", Engineering Fracture Mechanics, 57, 301-318 (1997).

[9] Addison, P.S, Mckenzie, W.M.C., Ndumu, A.S., Dougan, L.T., Runter, R., "Fractal cracking of concrete: parameterization of spatial diffusion", Journal of Engineering Mechanics, 125, 6, 622-629 (1999).

[10] Yan, A., Wu, Ke-Ru, Zhang, D., Yao, W., "Effect of the fracture path on the fracture energy of high-strength concrete", Cement and Concrete Research, 31, 1601-1606 (2001).

[11] Issa, M.A., Islam, Md.S., Chudnovsky, A., "Fractal dimension – a measure of fracture roughness and toughness of concrete", Engineering Fracture Mechanics,70, 125-137 (2003).

[12] Van Vliet, M.R.A, Van Mier, J.G.M., "Effect of strain gradients on the size effect of concrete in uniaxial tension", International Journal of Fracture, 95, 195-219 (1999).

[13] Vasconcelos, G., "Experimental investigations on the mechanics of stone masonry: characterization of granites and behavior of ancient masonry shear walls", Phd Thesis, University of Minho (2005).

[14] Costa, M.F.M., "Surface inspection by an optical triangulation method", Optical Engineering, 35, 2743-2747, 1996.

[15] Avdelidis, N.P., Delegou, E.T., Almond, D.P., Moropoulou, A., "Surface roughness evaluation of marble by 3D laser profilometry and pulsed thermography", NDT&E international, 37, 571-575, 2004.